Mon. Not. R. Astron. Soc. **311**, 541–554 (2000)

Three quasars from a survey of strong 25-μm emitters

R. D. Wolstencroft,[1] Q. A. Parker,[2★] C. J. Lonsdale[3] and S. M. Scarrott[4]
[1]*Royal Observatory, Edinburgh EH9 3HJ*
[2]*Anglo-Australian Observatory, PO Box 296, Epping, NSW 2121, Australia*
[3]*IPAC, California Institute of Technology, California 91125, USA*
[4]*Department of Physics, University of Durham, Durham DH1 3LE*

Accepted 1999 September 1. Received 1999 September 1; in original form 1998 December 14

ABSTRACT

We have carried out a spectroscopic survey of 750 sources that are strong 25-μm emitters from the *IRAS* Faint Source data base. Many of these sources are previously unknown active galactic nuclei including new *IRAS* quasars, three of which we describe here: F21382−2659, Z06367−6845 and Z05558−5008. They are all radio and X-ray quiet, and compared to the known *IRAS* quasars they have similar 25-μm luminosities, $L(25\,\mu\mathrm{m})$, but lower values of $L(25\,\mu\mathrm{m})/L(B)$. Their $F(25\,\mu\mathrm{m})/F(60\,\mu\mathrm{m})$ *IRAS* colours lie in the range 0.33 to 1.08, indicating the presence of relatively warm dust, presumably in a dusty torus surrounding the central source, and with temperatures similar to those of the known *IRAS* quasars. The quasar with the warmest dust, F21382−2659, exhibits broad (full width at half-maximum $\sim$4000 km s^{-1}) asymmetric Balmer lines with Hγ having an opposite asymmetry to the other broad lines; also Hβ (only) is double-peaked. Fe II is very weak in F21382−2659 but strong in the other two quasars, and the anticorrelation between Fe II and [O III] holds as anticipated. Two of the quasars are unpolarized: although F21382−2659 is optically polarized (2.1 per cent at 4950 Å), we argue that this provides little insight into the orientation of its dust torus relative to the line of sight.

Key words: galaxies: fundamental parameters – quasars: emission lines – quasars: individual: Z05558−5008 – quasars: individual: Z06367−6845 – quasars: individual: F21382−2659 – infrared: galaxies.

1 INTRODUCTION

Attempts to improve our understanding of the physics of active galactic nuclei (AGNs) by fitting all types of AGN into a genuinely unified scheme have so far been only partially successful. Although it is evident that the standard axisymmetric model AGN must differ greatly in appearance when viewed from different directions, the task of reconciling observation and model prediction is made difficult by the absence of an accepted view of how AGNs form and evolve. The two main sources of the anisotropy, namely the dusty obscuring torus and the radio jet with its radio lobes, undoubtedly evolve, probably on different time-scales, and are observed at differing phases of their evolution. Moreover, the host galaxies of the highest-luminosity AGNs, the quasars, appear to influence the radio properties of the quasars, with the radio-loud quasars (RLQs) always found in ellipticals and the radio-quiet quasars (RQQs) almost always found in spirals. It is therefore not surprising that the many complex phenomena observed in AGNs have not yet been fitted into a flexible and realistic unified scheme (e.g. see reviews by Antonucci 1993; Urry & Padovani 1995).

It is widely acknowledged that the selection of complete samples of AGN are crucial to tests of a realistic unified scheme, and that the problem of selection effects is in practice very difficult to avoid completely (Urry & Padovani 1995). In the case of radio-quiet AGN the need to have a selection criterion that is as immune as possible from the effects of obscuration is paramount. Selection on the basis of ultraviolet (UV) excess, for example, has often been used in the past; however, attenuation by the dust torus can be large, and in the case of type 2 Seyfert galaxies typically only 1 to 10 per cent of the central UV continuum source is seen, via scattering into the line of sight, thus discriminating against all but the most luminous type 2 Seyfert galaxies. Radiation that is isotropic and is scarcely affected by the torus, such as the mid- and far-infrared, radio continuum or hard X-ray bands, provides a better basis for selection in flux-limited surveys

In this paper (Paper I) and a companion paper (Paper II) we describe a large survey of sources taken from the *IRAS* Faint Source data base whose aim has been to establish the nature and number of AGN that are strong emitters at 25 μm. The rationale for this survey is our belief that many AGNs, especially those that

★ On special leave from the Royal Observatory, Edinburgh.

are relatively dust-rich, may have been missed in surveys at other wavelengths. The high likelihood that the 25-μm emission from these sources is relatively isotropic and the fact that the data base of 25-μm emitters is large (~114 000) have been particular incentives for us to carry out this survey. Our choice of 25 μm as the criterion, or more specifically the ratio $R = F(25\,\mu\text{m})/F(60\,\mu\text{m})$, is based on the early work of Miley, Neugebauer & Soifer (1985); de Grijp et al. (1985), who showed that R is typically 0.2 to 0.5 for Seyfert galaxies compared to 0.05 to 0.2 for galaxies whose central emission comes primarily from star formation. In a survey of 563 sources with $0.25 < R < 1.00$ taken from the *IRAS* Point Source Catalogue, de Grijp et al. (1992) found that 354 are galaxies and of these 62 per cent are AGN, with the fraction of AGN rising as R increases. The range of R values for the known *IRAS* quasars, i.e. quasars discovered by virtue of IRAS source follow-up, is relatively broad: for the 10 *IRAS* quasars listed by Clowes, Leggett & Savage (1991), $R = 0.23$ to 1.06 with $\langle R \rangle = 0.50$.

The connection between strong 25-μm emission and an active nucleus is widely thought to be via the thermal emission from the dust in the obscuring torus, heated to temperatures near to and up to sublimation by the nuclear source; models have been developed with inner radii as small as a few parsecs and outer radii of several hundred parsecs. Pier & Krolik (1992, 1993) have compared the properties of highly optically thick models of compact tori with spectral energy distributions (SEDs) of warm *IRAS* galaxies. In these models the torus is both hotter and more luminous when viewed face-on versus edge-on; however, they predict SEDs in the infrared that are too narrow. More realistic modelling of the size distribution and composition of the dust, as well as of the torus geometry and radiative transfer (Granato & Danese 1994; Efstathiou & Rowan-Robinson 1995), show better agreement with the observations, although it seems that some allowance for clumpiness of the torus material may still need to be made. Statistical evidence that dust in the narrow-line region (NLR) also contributes to the mid-infrared emission is discussed by Keel et al. (1994).

2 THE SURVEY

There are ~114 000 sources in our data base of strong 25-μm emitters, of which we have so far spectroscopically observed a sample of 750, using the 1.9-m SAAO Cassegrain spectrograph and the FLAIR multi-fibre system on the 1.2-m UKST at the AAO (e.g. Parker 1997).

Some statistics of the objects in our spectroscopic survey are given in Table 1. The sample selection was unbiased in the 10 FLAIR fields studied (three in 1992 and seven in 1994), but was biased towards higher values of $R = F(25\,\mu\text{m})/F(60\,\mu\text{m})$ in the SAAO study. A histogram of the B-band luminosities of the galaxies in the survey indicates a range $-16 > M(B) > -26$ with a main peak at about -20 and a lesser peak at about -23. At least 12 of the SAAO objects and 20 of the FLAIR objects are quasars based on both their luminosities and spectra, most of which show strong, broad Balmer lines and strong forbidden lines. Statistics on the spectral classification of the survey galaxies are given in Table 1. The AGN and quasar content of the survey as a whole will be discussed in detail in Paper II (Parker et al., in preparation).

None of the quasars so far discovered amongst the AGN in our survey are in existing catalogues. These *IRAS* quasars are distinctly different from the quasars discovered in surveys based on other frequency bands as we shall illustrate below. In this paper (Paper I) we have chosen three quasars to illustrate the type of quasar to be found in our survey. They were discovered early on in the survey and were the first to be followed up: we have no reason to believe that they are in any way unrepresentative of the quasar population of the survey. The companion paper (Paper II) will describe the full survey in detail (Parker et al., in preparation).

Table 1. Top: Statistics of the spectroscopic survey of 25-μm objects. Bottom: Spectral classification of galaxies in the survey. Key: GA, absorption lines only; GF, strong [O III], weak or absent Hβ; GB, strong broad Balmer emission lines; GN, narrow [O III] and Balmer emission lines; GC, composite spectrum.

Instrument	Year	No. objects	Galaxies	z(max)	$z > 0.1$
FLAIR	1992	91	45%	0.35	13%
SAAO 1.9-m	1992/93	150	51%	0.49	21%
FLAIR	1994	505	68%	0.17	7%
Type	GA	GF	GB	GN	GC
Fraction	4%	10%	29%	47%	10%

3 OBSERVATIONS

The coordinates of the optical counterparts of the three newly discovered quasars and their flux densities are listed in Table 2.

The hottest of the three, IRAS F21382−2659, is similar in a number of respects to the first *IRAS* quasar discovered, IRAS 13349+2438 (Beichman et al. 1986), as we show below. For this object we have carried out more extensive observations than on the other two – namely optical and near-infrared spectroscopy, *JHK* photometry, optical polarimetry and radio continuum measurements.

3.1 IRAS F21382−2659

The field centred on the *IRAS* source position is shown in Fig. 1. Optical identification was established using the likelihood ratio technique (Wolstencroft et al. 1986; Conrow et al. 1993): it is the brightest of four objects lying along an arc oriented approximately north–south. Gaussian profiles fitted to these objects indicate that three of the objects are stars with the quasar image being slightly extended (3 arcsec full width at half-maximum, FWHM). The optical counterpart has a B_J magnitude of 14.6(0.3) and it has a faint companion 3 arcsec to the NNW. The bracketed number in this and all subsequent cases where such brackets are used is an indication of the error. This magnitude estimate was obtained from

Table 2. Optical source positions and flux densities for the three new *IRAS* quasars.

IRAS ID	Optical position (J2000) RA and Dec.	Flux densities (Jy) $F(12)$	$F(25)$	$F(60)$	$F(100)$	R $F(25)/F(60)$
Z05558−5008	$05^h57^m04^s.2, -50°08'22''$	<0.06(0.02)	0.09(0.02)	0.16(0.14)	<0.36	0.56
Z06367−6845	$06^h36^m25^s.6, -68°48'22''$	0.05(0.02)	0.06(0.02)	0.18(0.03)	0.54(0.05)	0.33(0.12)
F21382−2659	$21^h41^m10^s.3, -26°45'51''$	0.23(0.02)	0.26(0.02)	0.24(0.03)	<0.50	1.08(0.16)

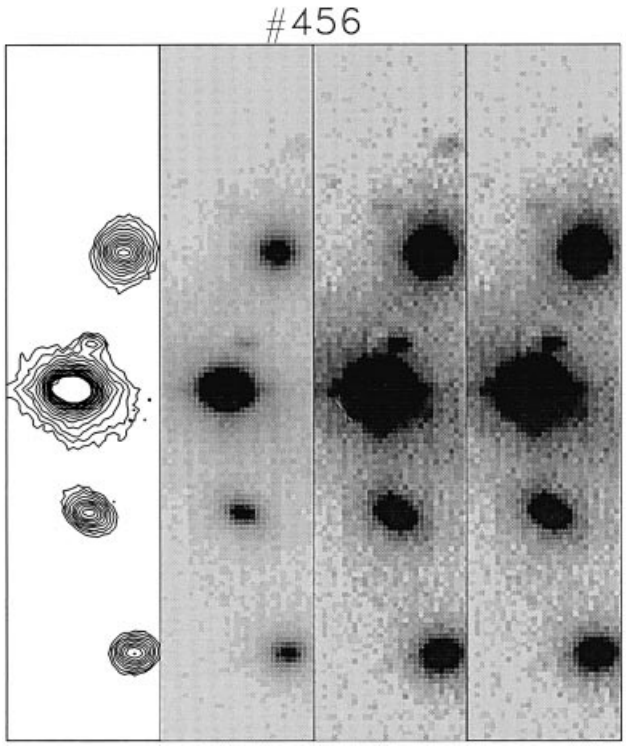

Figure 1. CCD image of the field of IRAS F21382−2659 taken with the Durham Imaging Polarimeter (*R* filter) mounted on the AAT in 1991 January. The image, shown at various contrast levels and in contour form, is oriented with north up and east to the left and is 9×43 arcsec^2. The quasar, the brightest of the four sources in the field, has a faint companion 3 arcsec to the NNW. The images are slightly trailed east–west, but it is possible to show that the quasar is slightly extended (3 arcsec FWHM) relative to the three other sources that are assumed to be point sources. The optical counterpart has RA = $21^h41^m10\overset{s}{.}26$, Dec. = $-26°45'50\overset{''}{.}9$(J2000).

the COSMOS Southern Sky Catalogue and is based on plate J8622 taken on 1983 June 12. *JHK* service photometry at UKIRT on 1991 November 4 using UKT9 yielded $J = 13.15(0.02)$, $H = 12.17(0.01)$ and $K = 10.88(0.01)$ in a 7.8-arcsec aperture: these colours ($J - H = 0.98$, $H - K = 1.29$) are typical of quasars (see e.g. Kotilainen et al. 1992).

The spectral energy distribution shown in Fig. 2 between 0.4 and 100 μm (Table 3) illustrates the similarity of IRAS F21382−2659 and 13349+2438. The distribution is very flat between 12 and 60 μm for both objects, which is probably related to the characteristics of the central nuclear source and the surrounding dust torus (see Wills et al. 1992). At a redshift of 0.129 (see below) IRAS F21382−2659 has an absolute magnitude $M(B) = -24.1$ and a far-infrared (FIR) luminosity (8–1000 μm) of $L(\mathrm{IR}) = 8.9(0.4) \times 10^{11}\,\mathrm{L}_\odot$ with $H_0 = 75\,\mathrm{km\,s^{-1}\,Mpc^{-1}}$, $q_0 = 0$, cf. $L(\mathrm{IR}) = 1.8(0.6) \times 10^{12}\,\mathrm{L}_\odot$ for IRAS 13349+2438.

3.1.1 *Optical spectroscopy*

We obtained a low-resolution (7-Å) discovery spectrum on 1990 December 14 in the range 3600–6500 Å using the Cassegrain spectrograph and Reticon detector on the 1.9-m SAAO telescope, which showed the object to be a quasar. Broad asymmetric Hβ and Hγ lines were evident with velocity widths (FWHM) ~4000 km s^{-1}, together with strong forbidden lines of [O III] 5007 Å, 4959 Å, [Ne III] 3968 Å and [Ne V] 3426 Å at a heliocentric redshift of 0.129. A striking feature of this spectrum was a very extended red wing of the Hβ emission-line profile, which appears rather abruptly at half the peak intensity. This red wing is not seen in the Hγ line, which has a rather steep red wing and a more tapered blue wing.

However, it is known that an Hβ asymmetry can arise because of Fe II blending (Jackson & Browne 1989), so that it is not possible to draw firm conclusions about the asymmetry from the original relatively low signal-to-noise ratio spectrum. We

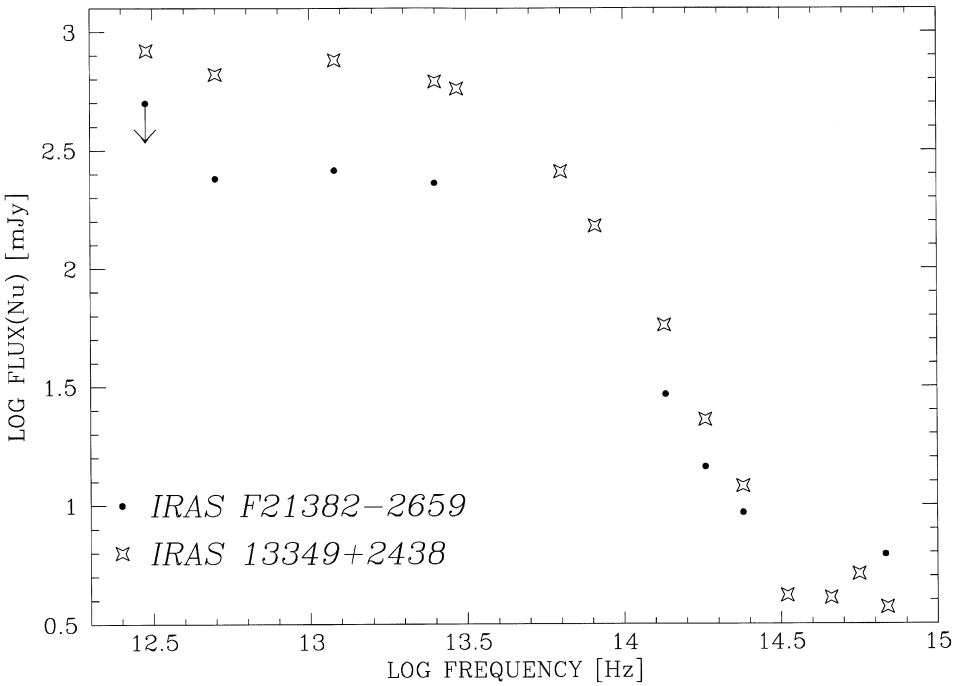

Figure 2. A comparison of the spectral energy distribution of IRAS F21382−2659 (Table 3) and IRAS 13349+2438 (taken from Wills et al. 1992).

therefore obtained an AAT high-resolution (1-Å) service spectrum (4650–5900 Å) with much improved signal-to-noise ratio on 1991 October 1, which is shown in Fig. 3. The strong red shoulder of the Hβ line is clearly seen. The absence of strong Fe II lines between Hβ and Hγ, where such lines are commonly observed (see e.g. Lipari, Macchetto & Golombek 1991), strongly suggests that the red asymmetry is real. The only significant line in this region appears to be He II 4686 Å observed at 5288 Å ($z = 0.1285$). The apparent weakness of Fe II and the strong [O III] in this object is consistent with the anticorrelation of Fe II and [O III] found by Boroson & Green (1992) in low-redshift quasars.

An important feature of the Hβ profile hinted at in the low-resolution and lower signal-to-noise ratio SAAO discovery spectrum is the double peak in the AAT spectrum at 5473.8 and 5488.0 Å. The latter line has the system velocity ($z = 0.1289$), with the other peak at $z = 0.1260$ being anomalous with a difference in velocity of 875 km s^{-1} (see Table 5). We might expect to see this double peak in the Hγ profile also (at 4887.4 and 4900.0 Å), but it is not apparent; note that [O III] 4363 Å is unlikely to make a detectable change to the Hγ profile given that the expected [O III] line ratio (4363):(5007+4959) is generally small, e.g. < 0.01 in the low-density limit (Osterbrock 1989). We also note that the low-noise AAT spectrum clearly confirms the blue asymmetry of the Hγ profile seen in the original lower-resolution SAAO spectrum (not shown).

A low-resolution (7-Å) follow-up spectrum of F21382−2659 covering 3800–7800 Å was obtained with the Cassegrain spectrograph and Reticon detector on the 1.9-m SAAO telescope on 1993 October 14 (Fig. 4, top). The expanded spectrum around Hβ (Fig. 4, bottom) reveals a double peak with a separation of 15.0 ± 0.8 Å, a result fully consistent to within the errors with the 14.2 ± 0.2 Å separation seen in the AAT spectrum and with comparable amplitudes for the two peaks. The region between [O III] 5007 Å and Hα is devoid of strong lines including Fe II. Hα shows a redward asymmetry similar to that of Hβ, which is easily seen in a higher-resolution spectrum taken around the line on 1993 October 18 (not shown). As for Hβ, the red shoulder appears to

Table 3. Spectral energy distribution of IRAS F21382−2659.

Wavelength (μm)	Magnitude	Flux density $F\nu$ (MJy)	ν (Hz)
0.44	$B_J = 14.6(0.3)$	6.2(1.7)	6.82×10^{14}
1.25	$J = 13.15(0.02)$	9.3(0.2)	2.40×10^{14}
1.65	$H = 12.17(0.01)$	14.5(0.1)	1.82×10^{14}
2.20	$K = 10.88(0.01)$	29.3(0.3)	1.36×10^{14}
12		230(20)	2.50×10^{13}
25		260(20)	1.20×10^{13}
60		240(30)	5.00×10^{12}
100		<500	3.00×10^{12}

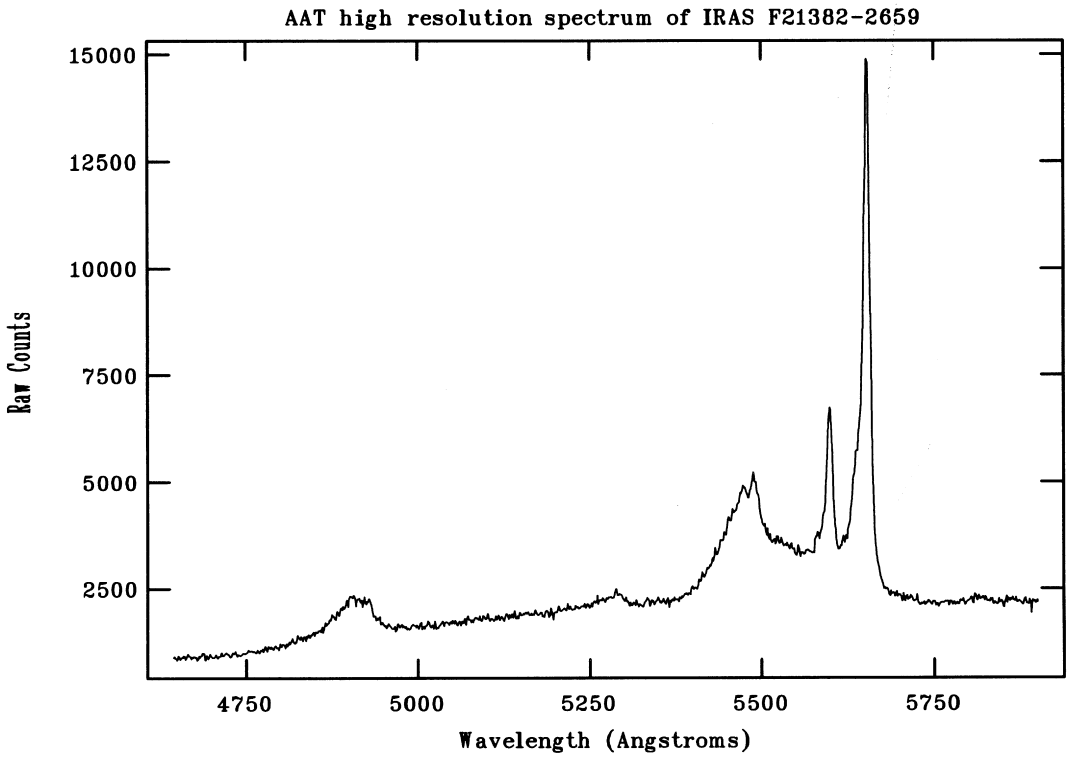

Figure 3. An AAT high-resolution (1-Å) service spectrum of IRAS F21382−2659 obtained with the RGO spectrograph on 1991 October 1 between 4650 and 5900 Å (the ordinate is counts). The spectrum shows Hγ and the Hβ, [O III] trio with He II 4686 Å appearing weakly from a region of weak Fe II lines; note the double-peaked Hβ line, which was first hinted at in the lower signal-to-noise ratio SAAO discovery spectrum in 1990 December; also note the line's strong red shoulder and the blue shoulder on the Hγ line.

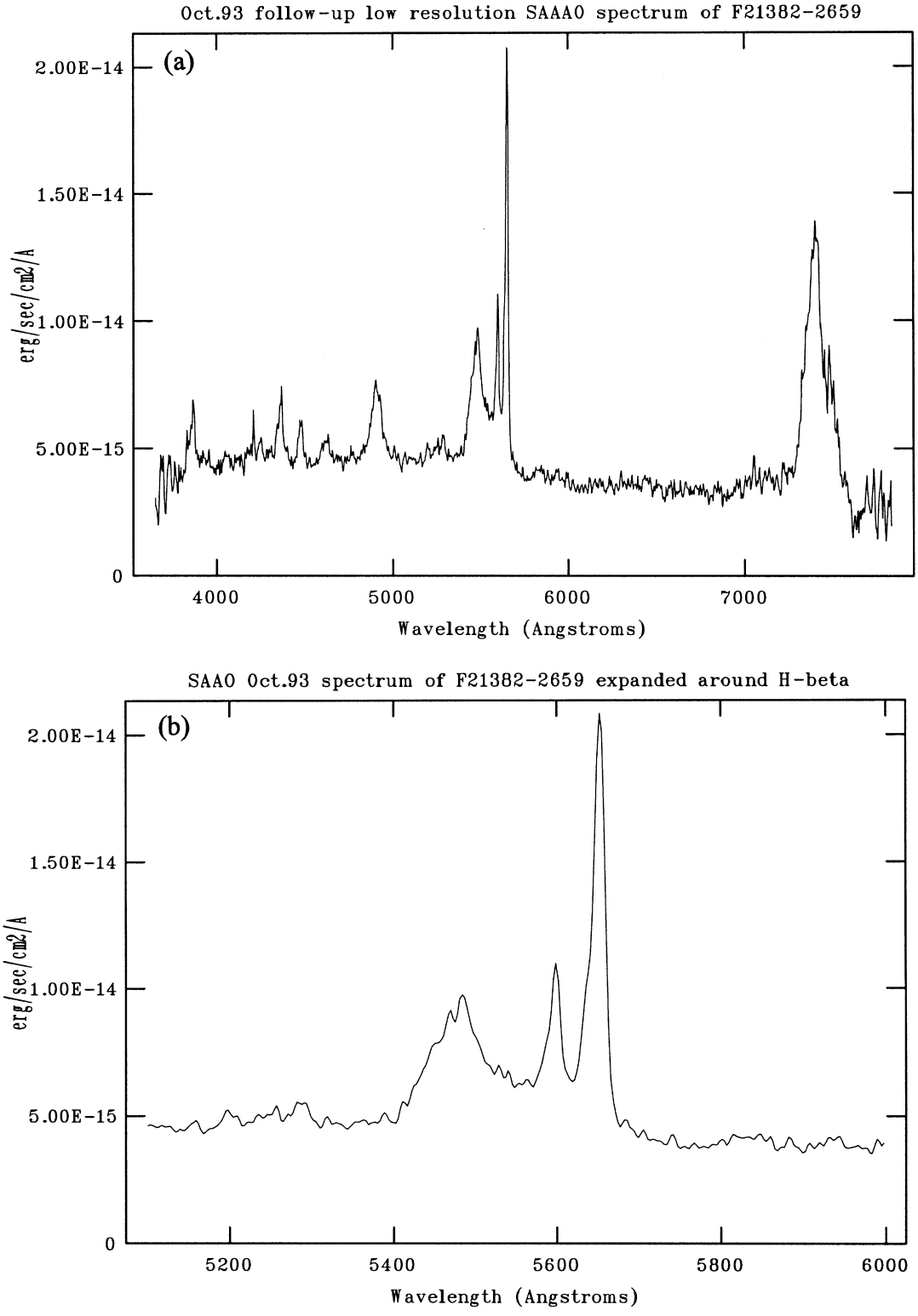

Figure 4. Top: Follow-up low-resolution, flux-calibrated spectrum of IRAS F21382−2659 covering 3800 and 7800 Å taken on 1993 October 14 with the Cassegrain spectrograph and Reticon detector on the SAAO 1.9-m telescope. The pronounced red shoulder on the Hα profile is readily apparent at this low resolution. Bottom: As above, but expanded about the Hβ, [O III] region where the double peak in the Hβ profile can be more clearly seen, as can the underlying red tail. A box 3 smooth was applied.

Table 4. Line properties from low-resolution follow-up SAAO 1993 October spectrum.

Identification	λ_{rest} (Å)	λ_{obs} (Å)	Redshift	Equiv. width (Å)
[Ne V]	3426	3860	0.1266	51(15)
[O II]	3727	4206	0.1285	21(16)
[Ne III]	3869	4359	0.1268	56(14)
[Ne III]	3969	4474	0.1273	38(10)
Hγ	4340	4905	0.1300	133(34)[a]
Hβ	4861	5483	0.1279	96(13)[a]
[O III]	4959	5597	0.1287	27(2)
[O III]	5007	5651	0.1287	76(7)
Hα	6563	7401	0.1277	343(10)

[a] Equivalent width values are uncertain.

Table 5. Line properties as measured from the higher-resolution AAT spectrum.

Species	Rest-frame λ (Å)	Observed λ (Å)	FWHM (Å)	Redshift
Hγ	4340.5	4908.1	60	0.1308
He II	4686.0	5284.7	43	0.1278
Hβ (left peak)	4861.3	5473.8	23	0.1260
Hβ (right peak)	4861.3	5488.0	20	0.1289
Hβ (full[a])	4861.3	5479.5	n/a	0.1272
[O III]	4958.9	5598.0	15	0.1289
[O III]	5006.8	5652.2	13	0.1289

[a] Based on best-fitting Gaussian to both peaks ignoring extended red shoulder.

start rather abruptly close to the half-maximum point of the profile. There is no sign of the double peak in the Hα profile, for which, extrapolating from the AAT spectrum of 1991 October, we would have expected peaks at 7389.7 and 7408.7 Å. A list of identifications, wavelengths and equivalent widths as measured from the SAAO and AAT spectra are given in Tables 4 and 5.

Possible origins for line asymmetry and for a double peak have been discussed by various authors. Double-peaked profiles are explained by Eracleous & Halpern (1994) in terms of line emission from an accretion disc viewed relatively edge-on but this is thought to apply primarily to radio-loud objects. IRAS F21382−2659 is a radio-quiet quasar (see Section 2.1.4) so it is not clear that this mechanism would apply. The difficulty in understanding the profiles of broad emission lines in terms of physical models has been emphasized by Robinson (1995a,b) and this of course applies especially to the interpretation of profile asymmetries. We will return to these topics in Section 4.

3.1.2 Near-infrared spectroscopy

Since Hβ and Hγ exhibit opposite asymmetries and arise from different atomic levels ($n = 4, 3$), we decided to examine the profile of Pα, which arises from the same level as Hβ, as well as the Hα profile (for which Fe II contamination should be less) in the hope that this might provide a clue to the origin of the asymmetries so far observed. A UKIRT service spectrum was also obtained using CGS4 on 1991 November 4, in the range 2.03–2.45 μm at a resolution of 0.0074 μm. The spectrum was sampled every one-third of a resolution element and calibrated using the ratio star BS 7231, an F6V star with $K = 5.8$ and whose temperature was assumed to be 6400 K; its Brγ absorption feature was artificially removed before dividing by it. The spectrum shown in Fig. 5 was smoothed with a Gaussian of FWHM 1.5 channels (0.5 resolution element). The dominant feature is Pα at 1.8751 μm with a peak wavelength of 2.1156 μm corresponding to $z = 0.1283$ and a prominent red shoulder, i.e. the same asymmetry as for Hα and Hβ. The equivalent width and linewidth of Pα are 0.0165 and 0.0405 μm respectively. The spectral resolution was not high enough to resolve the double peaks inferred from the 1991 October Hβ observation at 2.1114 and 2.1168 μm.

At the edge of the spectral window, a narrow line at 2.449 μm coincides with Brγ at $z = 0.1309$. The broad asymmetric feature at 2.21 μm (Fig. 5) is almost certainly a blend of H_2 ($v = 1$–0) S(3) at 1.9576 μm and [Si VI] 1.9615 μm, which has been observed in Seyfert galaxies such as NGC 1068 (Moorwood & Oliva 1994) and in Cygnus A (Ward et al. 1991). The ratio of the line flux in the [Si VI] line to that of the S(3) line is 4 ± 2 for NGC 1068 and Cyg A. In the case of IRAS F21382−2659 the ratio is probably higher since the H_2 ($v = 1$–0) S(1) 2.121-μm line is not detected at the expected wavelength of 2.392 μm and the ratio 2.121-μm S(1)/1.958-μm S(3) is 1.0 (NGC 1068) or 1.5 (CygA). The red asymmetry of this feature is thus most probably related to the red asymmetry of the broad Balmer and Paschen lines rather than to any blending as for Cygnus A (see Ward et al. 1991). Note that the presence of this line indicates the presence of very energetic ionizing photons with $h\nu > 167$ eV. A line that we might have expected to see such as Brδ (1.9446 μm), which should be seen at 2.1940 μm, is not detected.

3.1.3 Optical polarimetry

Polarization in quasars and AGNs is in general attributed to either synchrotron radiation or scattering of radiation from the central source obscured by a dusty torus. While this latter picture is normally seen to be applicable to those type 2 Seyfert galaxies whose broad lines are only seen in the spectrum of the polarized

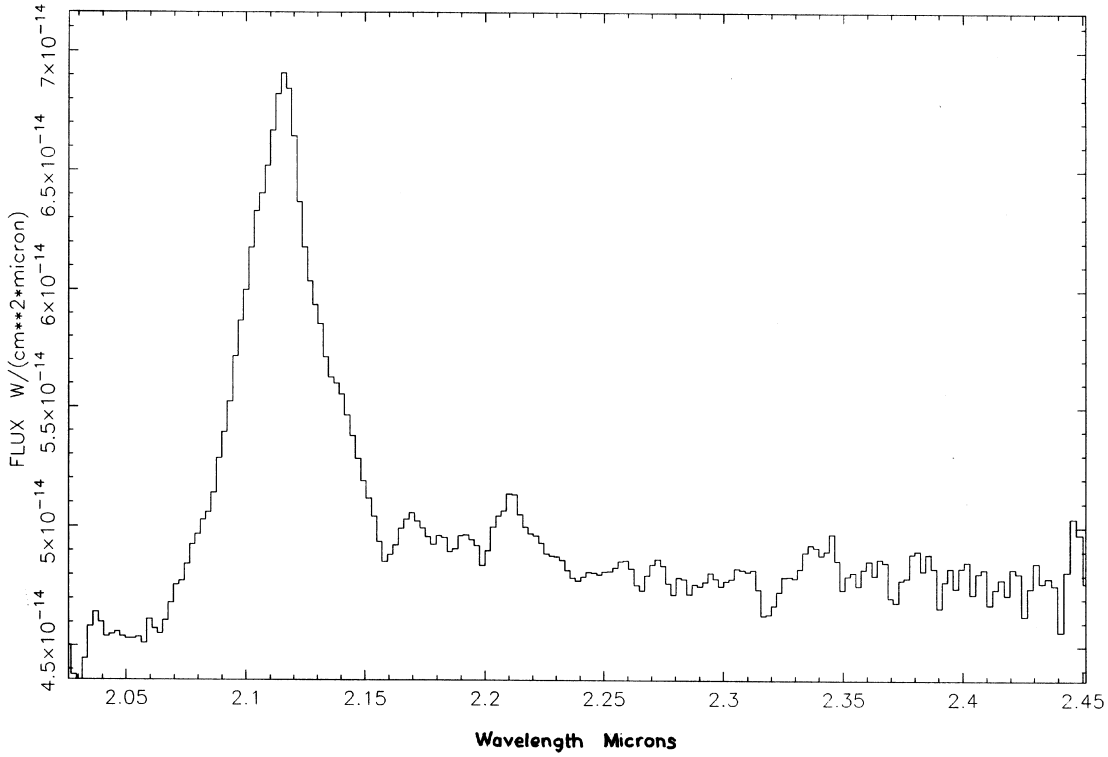

Figure 5. A UKIRT service spectrum of IRAS F21382−2659 between 2.03 and 2.45 μm using CGS4 at a resolution of 0.0074 μm taken on 1991 November 4. The main emission line, Paschen α, shows a prominent red shoulder. The broad feature at 2.21 μm is very probably a blend of H_2 ($v = 1$–0) S(3) and [Si VI] at rest wavelengths of 1.9576 and 1.9615 μm respectively.

flux, it may also apply to certain quasars, and Wills et al. (1992) have made a good case for IRAS 13349+2438 fitting this picture and for it to be categorized as a type 2 quasar. It seems plausible to suppose that *IRAS* quasars are likely as a class to possess considerable amounts of dust and to contain other examples of type 2 quasars.

Imaging polarimetry of IRAS F21382−2659 was carried out using the Faint Object Polarimeter on the AAT on 1994 July 24 (we are indebted to Gavin Ramsay and Mark Cropper who made these observations). The polarization was measured in two bands using OG570 and BG39 Schott filters, which, together with the response of the thinned Textronic charge-coupled device (CCD) chip, defined effective wavelengths of 7300 and 4950 Å with FWHM ranges of 5750–8900 Å and 3700–6150 Å, respectively. The results are summarized in Table 6: the chip was binned 2 × 2 to provide 0.84 arcsec per binned pixel.

As the quasar is at galactic coordinates $l = 22$, $b = -48$, well outside the plane, the interstellar polarization should not be large. Of six stars within 5 deg listed in the catalogue of Mathewson & Ford (1970), all have observed polarization p in the range 0.04 to 0.40 per cent, with no discernible preferred position angle, $m - M$, between 4.7 and 12.0 deg and $0.0 < A(V) < 0.5$. The averaged $p/A(V)$ of 0.38 per cent/mag at $\theta = 92$ deg indicates that the interstellar component of p is most probably no greater than 0.2 per cent and can be disregarded.

The polarization of IRAS 13349+2438 (a known quasar) rises towards shorter wavelengths ranging from 3.3 per cent at 8000 Å to 8.0 per cent at 3600 Å (Wills et al. 1992). These data can be well fitted to a power law, viz. $\ln(p) = n \times \ln(\lambda) + C$, with $n = 1.12$ and C a constant. If we fit our two observations of IRAS F21382−2659 to a power law, we obtain $n = 1.04$, from which we may extrapolate a value $p = 3.0$ per cent at 3600 Å. While the position angle of IRAS 13349+2438 is constant with wavelength in the visible, there is a small but significant rotation in θ for IRAS F21382−2659, which might indicate that two competing processes are responsible for the polarization. The observed position angle bears no obvious relation to the direction of the faint companion at 19 deg west of north. The red and blue images obtained with the polarimeter both indicate that the host galaxy is extended approximately north–south, and again this has no plausible connection to the observed position angle.

Table 6. Polarization measures for quasar IRAS F21382−3659.

Filter	Wavelength (Å)	p (per cent)	θ (deg)
BG 39	4950 (3700–6150)	2.13(0.19)	57.4(2.6)
OG 570	7300 (5750–8900)	1.42(0.12)	48.7(2.5)

3.1.4 X-ray and radio observations

IRAS F21382−2659 was observed with the *ROSAT* sky survey instrument (PSPC): 11 counts were registered in 368 s, i.e. 0.030 photon s^{-1} in the energy range 0.1–2 keV (Voges, private communication). The hardness ratio of −0.50(0.50) is poorly determined but it is certainly a soft source: with an average photon energy of about 0.5 keV this corresponds to a flux of 2.4×10^{-11} erg s^{-1}, and hence to a flux density of 6.0×10^{-14} erg cm^{-2} s^{-1}. Although at a similar distance, IRAS 13349+2438 ($z = 0.107$) has a much greater count rate (2.483 photon s^{-1}) and has an X-ray luminosity ~60 times larger: it is also a soft source with hardness ratio −0.49. If the two

quasars were objects similar in central luminosity, torus geometry and scattering properties, but just viewed at differing angles, we would interpret the higher polarization of IRAS 13349+2438 as a result of viewing the central source through the dust torus more nearly edge-on. If so, the soft X-rays would be more strongly attenuated in IRAS 13349+2438 and the intrinsic X-ray luminosity would be even greater. Unless one or both sources are highly variable in the *ROSAT* PSPC band, either the geometry of the torus or the central luminosity, or both, are quantitatively different.

Radio observations of IRAS F21382−2659 were made on 1993 May 30, with the Molonglo (MOST) telescope at 843 MHz. There was no detection: the 3σ upper limit to the flux density was 10 mJy.

3.2 IRAS Z05558−5008

Of the three sources listed in Table 1, IRAS Z05558−5008 is intermediate in flux density and in its R value (0.56). We identify it with a $B_J = 16.3$ point source (see Fig. 6). Spectroscopy of the source, carried out with the FLAIR multi-object spectrograph on 1992 January 2, showed it to have a redshift of 0.355, thus making it a quasar with $M(B) = -24.8$, slightly more luminous optically than IRAS F21382−2659.

The low-resolution FLAIR spectrum between 3900 and 7300 Å is shown in Fig. 7. [O III] 5007 and 4959 Å plus Hβ are prominent, and Hγ and [O II] 3727 Å are also apparent. The nature of the deep troughs either side of the Hβ [O III] lines is unclear. A low-resolution (7-Å) spectrum taken on 1997 February 13 using the 1.9-m SAAO telescope with the Cassegrain spectrograph and Reticon detector indicates the presence of strong iron lines between Hβ and Hγ and beyond 5007 Å. The trough shortward of Hβ seen near 4725 Å (rest) in the FLAIR spectrum may be similar to that seen in the *IRAS* AGNs with extreme Fe II emission studied by Lipari, Terlevich & Macchetto (1993); in the SAAO spectrum this is seen to be a complex region and also to contain He II 4686 Å in emission. Likewise the trough longward of [O III] 5007 Å is seen to lie shortward of the strong Fe II lines peaking near 5250 Å. The other lines revealed in the SAAO spectrum are the neon lines [Ne V] 3426 Å and [Ne III] 3869 and 3968 Å. Although the spectrum extends down to a rest wavelength of 2500 Å, the presence of the Mg II 2798 Å line is difficult to assess because of the noise.

Z05558−5008 was not detected in the *ROSAT* PSPC sky survey, which indicates an upper limit in the energy range 0.1–2 keV of about 3×10^{-14} erg cm^{-2} s^{-1}. To our knowledge neither has it been detected in any of the radio continuum surveys of the southern sky currently in progress, which indicates that it is a radio-quiet object.

Finally, the polarization of Z05558−5008 was measured through a broad V filter using the Durham Imaging Polarimeter on the 1-m SAAO telescope on 1997 February 13. No significant polarization was detected ($p = 0.4 \pm 0.5$ per cent).

3.3 IRAS Z06367−6845

IRAS Z06367−6845 is another example of a quasar found in the so-called reject file, which contains the lowest signal-to-noise ratio objects in the *IRAS* Faint Source Database (FSDB). As they represent 77 per cent of all the 760 000 sources of the FSDB, it is important to know what fraction are real sources: this question is addressed in Paper II. The effective *IRAS* integration time for Z06367−6845 was relatively long since it lies close to the south ecliptic pole; however, it also lies on the fringes of the Large Magellanic Cloud (LMC) so that source confusion can affect the signal-to-noise ratio. Note that the quasar Q0637−752 is also seen through the LMC and that it was shown by Bowen, Blades & Pettini (1995), using GHRS on phHST, to exhibit strong Mg II absorption lines associated with gas in the LMC: this may also be the case for Z06367−6845. After co-addition, Z06367−6845 is detected in all four bands with flux densities of 0.06 and 0.18 Jy at 25 and 60 μm respectively and an R value of 0.33 (see Table 2).

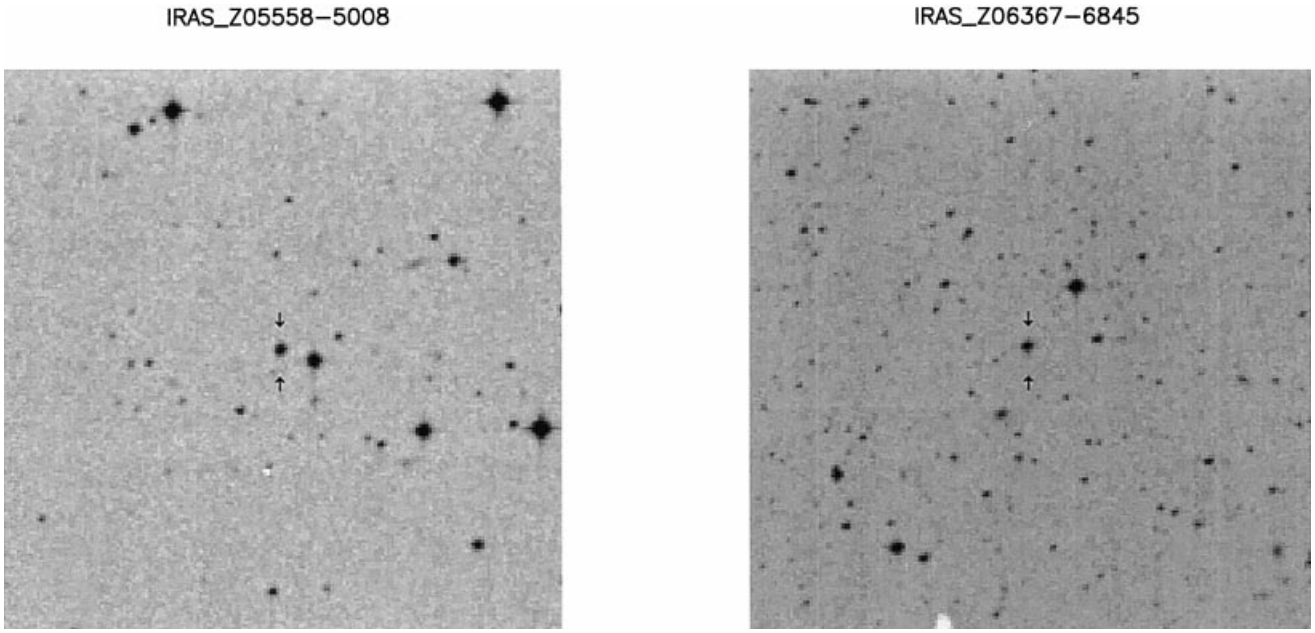

Figure 6. Finding charts (5×5 arcmin^2) of IRAS Z05558−5008 and Z06367−6845 taken from the Digital Sky Survey.

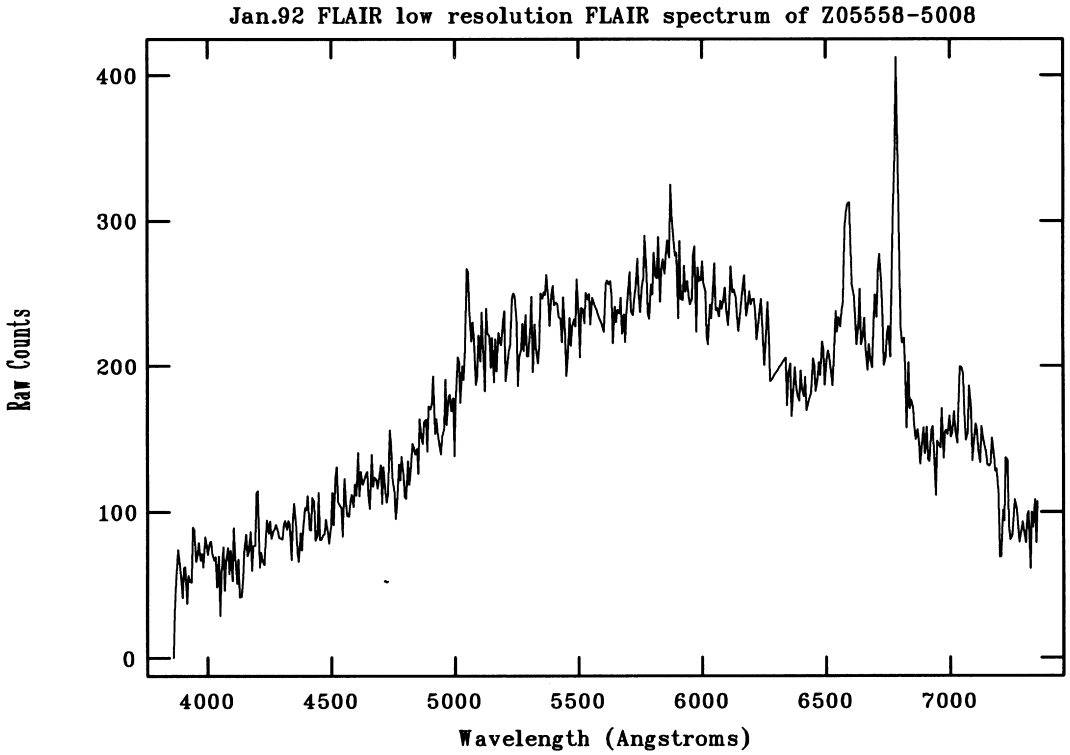

Figure 7. Spectra of Z05558−5008 taken with the FLAIR multi-object spectrograph on the UK Schmidt telescope on 1992 January 2 between 3900 and 7300 Å (the ordinate is counts). Sky lines at 5577 and 6300 Å were not adequately fully removed and so the spectrum has been interpolated across the residual signal.

Despite the high image density the *IRAS* source was unambiguously identified with a $B_J = 16.0$ object: imaging with the AAT in 1994 March (Fig. 8) shows that it is slightly extended (4 arcsec full width zero intensity, FWZI) and elongated on its west side. At fainter contour levels a southern extension is apparent. Fig. 9 shows a finding chart for this crowded field towards the edge of the LMC. Near-infrared photometry, carried out on the SAAO 1.9-m telescope on 1997 February 24, yielded $K = 12.98(0.03)$, $H = 14.09(0.08)$, $J = 15.0(0.2)$.

A low-resolution (7-Å) spectrum obtained on 1992 March 8 with the Cassegrain spectrograph and Reticon detector on the 1.9-m SAAO telescope (Fig. 10) shows strong lines of Hβ, Hγ and Mg II 2798 Å at a radial velocity of 100 850(900) km s^{-1}, i.e. at a redshift of 0.336. The FWHM velocity width of Hβ is 3000 km s^{-1}. The corresponding $M(B) = -25.0$ makes this the most optically luminous of the three quasars. Although [O III] 5007 Å is visible, it is weak. Broad features between Hβ and Hγ and redward of [O III] 5007 Å are most plausibly identified with the Fe II bands seen also in IRAS F05558−5008. The relative strengths of [O III] 5007 Å and these Fe II bands are in accord with their anticorrelation noted by Boroson & Green (1992).

The polarization of Z06367−6845 was measured with the Durham Imaging Polarimeter (Scarrott et al. 1983) at the Cassegrain focus of the AAT in 1994 March. No polarization was detected, with the formal value being $p = 0.825(1.022)$ per cent at a position angle $\theta = 85(35)$ deg (no filter).

ROSAT did not detect this source during the course of the *ROSAT* sky survey (Voges, private communication) despite the favourable ecliptic latitude. Deeper pointed observations of the LMC have been made with *ROSAT* (Pietsch, private communication), including this direction, but there was no detection, indicating an upper limit of about 0.01 count s^{-1} in the 0.1–2 keV band corresponding to a flux density upper limit of 2×10^{-14} erg cm^{-2} s^{-1}.

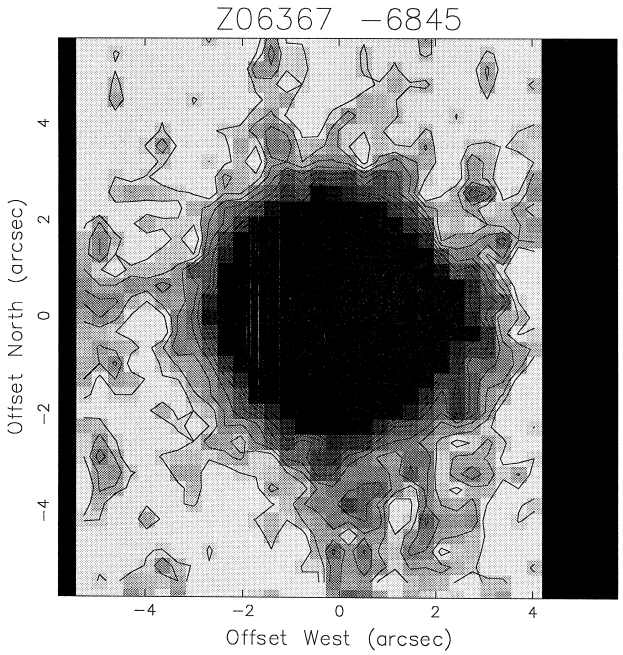

Figure 8. An image of Z06367−6845 (*R* filter) taken with the AAT in 1994 March. It is slightly extended (4 arcsec FWZI) and has a faint southerly extension.

4 DISCUSSION

The redshifts, magnitudes, luminosities and colours are listed for the three newly discovered *IRAS* quasars in Table 7. They are similar in that they are all radio quiet and X-ray quiet and they contain appreciable amounts of warm dust, which we presume is distributed in a torus surrounding each central engine. We assume that the paradigm for less dusty quasars applies also to *IRAS* quasars, namely that the inclination of the line of sight to the plane of the torus is the main factor governing whether we see broad lines and how much of the radiation we see reaches us directly, though attenuated, rather than via scattering. The optical polarization provides a measure of the importance of scattering and, in principle, the inclination of the torus to the line of sight. The strength of the iron lines can be quite strong in *IRAS* quasars: if some of this gas is generated close to the innermost surface of the torus where dust is thought to sublime, then the viewing geometry, X-ray luminosity and iron line strength could be interrelated. In the discussion below we consider what support our data give to the picture painted above.

4.1 Broad-line profiles in IRAS F21382−2659

The most puzzling aspects of the observations described in

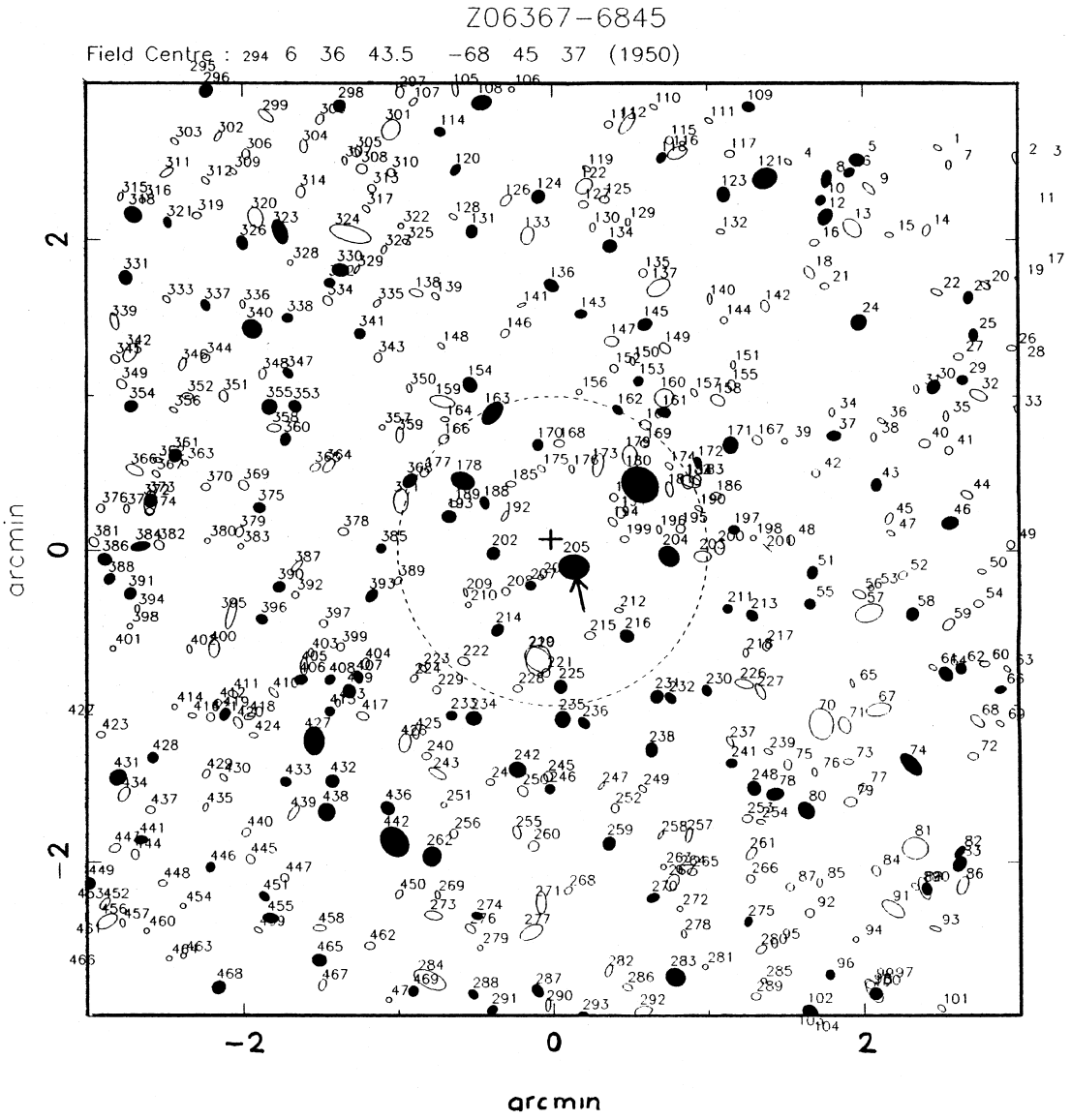

Figure 9. Finding chart for Z06367−6845 produced using the *IRAS* identification package based on COSMOS measurements of the UK Schmidt southern sky survey (Conrow et al. 1993). The field centre is marked with a cross and the *IRAS* ID with an arrow.

Table 7. Luminosities for the three new *IRAS* quasars.

IRAS	z	B_J	K	$M(B)$	$L_{FIR}/L(0)$	$L_{FIR}/L(B)$	$F(25\,\mu m)/F(B)$
Z05558−5008	0.355	16.3	–	−24.8	$2.1(0.9)\times10^{12}$	3.0(1.2)	70
Z06367−6845	0.336	16.0	12.98	−25.0	2.7×10^{12}	3.1	35
F21382−2659	0.129	14.6	10.88	−24.1	$8.9(0.4)\times10^{11}$	2.3(0.1)	42

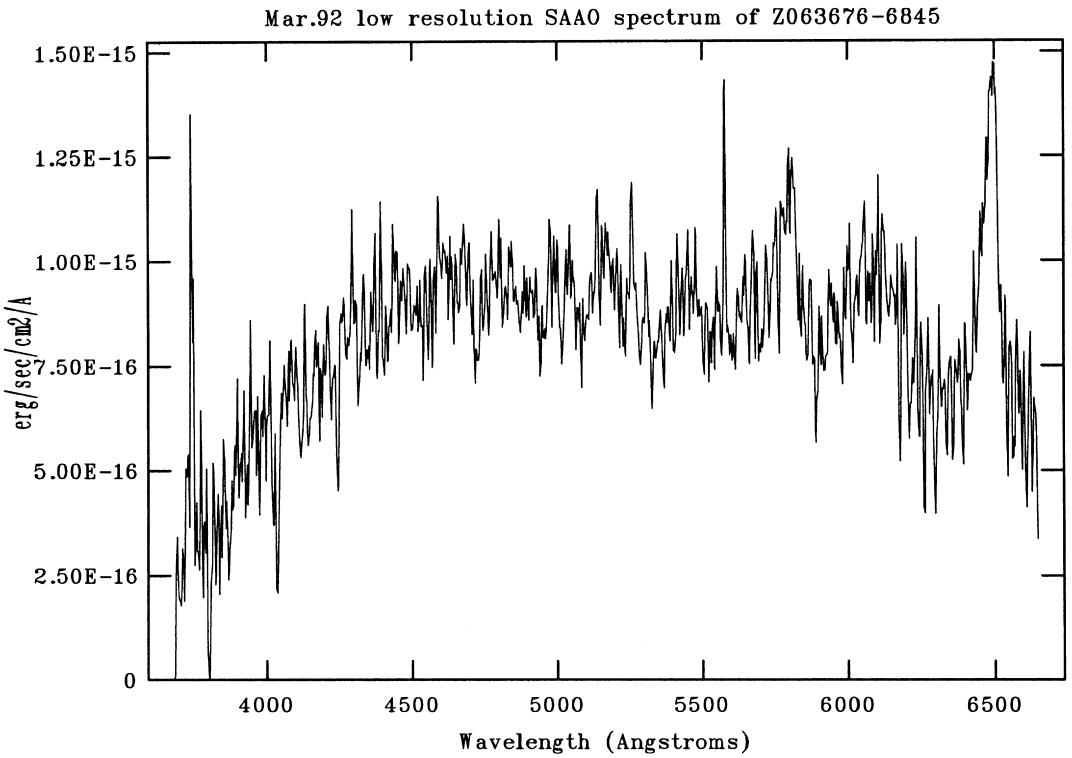

Figure 10. A low-resolution (7-Å), flux-calibrated spectrum of IRAS Z06367−6845 taken on 1992 March 8 with the Cassegrain spectrograph and Reticon detector on the 1.9-m SAAO telescope. Strong Fe II lines are seen between Hβ and Hγ, and Mg II 2798 Å is seen.

Section 3 are: first, the asymmetry of the broad emission lines, which differs between lines; and secondly, the double peak seen in Hβ but not in Hα or Hγ, although the resolution was adequate to reveal such a double feature. We also note that the linewidths differ between lines, with Hβ and Hγ having smaller values (FWHM = 4047, 4141 km s^{-1}) than Hα and Pα (FWHM = 5316, 5406 km s^{-1}. Differences in the simultaneously observed profiles of the broad hydrogen lines in individual AGNs have been reported by many authors (e.g. Shuder 1982, 1984; Stirpe 1990). Also the monitoring of AGN line profiles indicates that they change with time in response to changes in the ionizing continuum (Peterson 1993). The distance of the emitting atoms from the central source and the overall geometry of the broad-line region affects the amount of ionizing radiation reaching the emitting gas and the emitted radiation reaching the observer in a manner that is difficult to model effectively. The width of the broad lines is usually attributed to a large population N of clouds with different velocities, each emitting narrow lines appropriate to $T \sim 10^4$ K (13 km s^{-1}), with N large enough ($> 10^4$) that the high-resolution profiles are still observed to be smooth rather than spiky. To accommodate recent extensive results of monitoring broad-line profiles in AGN, photoionization models have been reassessed by Shields, Ferland & Peterson (1995), who suggest that there are two populations of broad-line clouds: namely those optically thin (to Lyman α), which are ionized throughout; and those optically thick, where the ionization is spatially limited to the side of the cloud facing the central engine.

Returning to the specifics of IRAS F21382−2659, we consider how the hydrogen line profiles can differ in width and asymmetry and in being double or single peaked. As we implied above, the individual clouds may in principle be infalling, outflowing, in Keplerian orbits or a combination of all three. In a recent analysis of NGC 5548, Done & Krolik (1996) , using the best available data on line profile and continuum variations, conclude that a significant component must involve radial infall; however, it is uncertain whether this might be true for AGN in general. Baldwin and his collaborators (Baldwin et al. 1995; Ferguson et al. 1997) have stressed that it is unrealistic to explain the entire emission-line spectrum as if it all came from the same cloud or set of clouds, and that the broad-line region (BLR) is almost certainly stratified with different lines arising in different groups of clouds. If this is indeed true, then we no longer need to be concerned about the differing properties of the lines in terms of one physical model, but each line can be modelled independently. One parameter of the main lines in IRAS F21382−2659 that is the same is the central wavelength. In particular, the average ($z = 0.1275$, 5481.1 Å) of the two peaks of Hβ at $z = 0.1260$ and 0.1289 (5473.8 and 5488.0 Å) agrees with that of Hα at $z = 0.1277$ (7401 Å) and Pα ($z = 0.1283$, 2.11562 μm) within the errors. This suggests that the kinematics of the clouds responsible for each line are not wildly different, and that weighting according to optical depth and radiative transfer are mainly responsible for line profile differences.

The double peak ($\Delta\lambda = 14.2 \pm 0.2$ Å) was clearly seen in Hβ in the high-resolution (1-Å) AAT spectrum (Fig. 3) and, although at lower resolution (7 Å), it was also seen ($\Delta\lambda = 15.0 \pm 0.8$ Å) in the 1993 October SAAO spectrum; in both cases the relative amplitudes as well as the separation of the two peaks were consistent. In the case of the 1990 December SAAO spectrum, the noise level was such that the presence of a double peak in Hβ could not be firmly established. As for the other Balmer lines where a double peak could have been readily detected if present (Hγ in Fig. 3 and Hα in Fig. 4 and the associated higher-resolution spectrum), it was not seen. As noted in the previous

paragraph, each Balmer line can be modelled independently according to Baldwin et al. (1995), so that the absence of a double peak in Hγ in the same spectrum in which Hβ was seen to be double (Fig. 3) may not present a problem. It is possible that the Hβ line may be variable, though further high-resolution spectroscopy is needed to establish this. It is worth noting that, although the double-peaked broad lines discussed by Eracleous & Halpern (1994) are found primarily in radio-loud AGN, a handful of radio-quiet AGN also show such double lines. In the case of the radio-quiet nucleus of NGC 1097, the broad Hα line has been double-peaked and variable since its abrupt appearance in 1990 (Storchi-Bergmann et al. 1995, 1997): these authors attribute this behaviour to emission from a precessing accretion disc in the nucleus.

4.2 Fe II emission

Optical Fe II emission is a common feature of AGN spectra. The Fe II line strength, normalized to that of Hβ, is typically R(Fe II) = Fe II 4570/H$\beta \sim 0.4$, with about 90 per cent falling in the range 0.1 to 1.0 (Lawrence et al. 1997). A small group of AGN with R(Fe II) well above unity are known and include several *IRAS* quasars such as IRAS 07598+6508 with $R = 2.5$ (Lawrence et al. 1988) and IRAS 18508−7815 with $R = 3.1$ (Lipari et al. 1991). A variety of correlations among quasar properties have been suggested in the Boroson & Green (1992) study of the Palomar–Green quasars. They find a strong anticorrelation of Fe II strength with [O III] strength and with the FWHM of Hβ. Further, in their recent study of a sample of AGN with a wide range of R(Fe II), Lawrence et al. (1997) point out a clear trend for strong Fe II emitters to be X-ray quiet. How well are these trends followed by our three *IRAS* quasars? We have estimated R(Fe II) by using the 4570 Å Fe II profiles (comprising multiplets 37 and 38) of the Boroson & Green (1992) spectra of low-redshift quasars. We obtain the mean value of R(Fe II) for the profiles that give the best fit to each of our three quasars, namely R(Fe II) = 0.8, 0.9 and 0.1 for Z05558−5008, Z06367−6845 and F21382−2659 respectively. Neither of the two sources with strong Fe II, Z05558−5008 and Z06367−6845, were detected in the *ROSAT* PSPC survey (< 0.01 photon s^{-1}), whereas F21382−2659, which is very weak in Fe II, was readily detected (0.030 photon s^{-1}) – in agreement with the expected trend. The stronger [O III] 5007 Å and broader Hβ for F21382−2659 also agree with the suggested correlations.

Can we draw any conclusions about the physics or geometry of the Fe II emitting regions from the trends described above? Further, does the polarization being significant only for the Fe II weak quasar F21382−2659 have any bearing on this question? Lawrence et al. (1997) point out that the anticorrelation of Fe II and [O III] strengths could be explained if a large part of the [O III] came from radii small enough for obscuration by the molecular torus to play a role, implying that weak [O III] and hence strong Fe II emitters are preferentially seen edge-on. If polarization is seen as being greatest when the torus is seen edge-on, then we would anticipate that the polarization would be weakest for F21382−2659, the opposite of what is observed. Perhaps the relation between the polarization and the inclination of the torus is more complex (see below).

4.3 Comparison with other low-redshift *IRAS* quasars

In Table 8 we list the main infrared and optical photometric properties, as well as optical polarizations where known, of 12 low-redshift ($z < 0.5$) *IRAS* quasars taken from the lists of Low et al. (1988, 1989) and Clowes et al. (1991), together with the properties of the three quasars discussed in the present paper. Histograms of the infrared luminosity, $L_{\rm IR} = L$(8–1000 μm), and optical absolute magnitude, $M(B)$, in Fig. 11, clearly show that the three quasars fall at the high end of the optical and the low end of the infrared luminosity distributions of the 12 quasars. In terms of the 25-μm luminosity, L(25 μm), we note that both samples have a similar distribution in L(25 μm) but have lower values of L(25 μm)/$L(B)$. Although one cannot infer much from such a small sample, it is true that the sample from which our three quasars are drawn is biased in favour of lower *IRAS* fluxes and warmer 25/60 colours, and observational selection effects are evidently involved. The influence of the 25-μm emission can be judged from Fig. 12, where the dependence of L(25 μm)/$L_{\rm IR}$ on $R = F$(25 μm)/F(60 μm) shows that 11 of the 12 quasars define a narrow sequence implying similarly shaped SEDs across

Table 8. Low-redshift *IRAS* quasars.

IRAS	z	B	F(60) (Jy)	R[a]	log($L_{\rm IR}$) ($L_\odot$)	$L_{\rm IR}/L(B)$	$M(B)$	$p(B)$ (per cent)	$L(25)/L_{\rm IR}$[b]
00275−2859	0.28	17.1	0.69	0.251	12.49L[c]	11.6L	−23.4	–	0.198L
04505−2958	0.286	16.0	0.65	0.290	12.62	6.8	−24.6	0.6	0.224
07598+6508	0.148	14.5	1.69	0.316	12.45	4.9	−24.5	2.5	0.222
09104+4109	0.442	18.5	0.53	0.635	13.11L	76L	−23.2	14.8	0.327L
09149−6206	0.057	13.6	2.46	0.484	11.81	3.6	−23.3	–	0.296
10479−2808	0.326	16.0	1.00	0.326	12.48	12	−23.6	–	0.228
12540+5708	0.042	14.0	31.99	0.271	12.49	46	−22.2	7.3	0.245
13218+0552	0.190	19.0	1.17	0.343	12.56	233	−20.8	–	0.222
13349+2438	0.108	15.1	0.61	1.375	12.23L	9.9L	−23.2	6.5	0.282L
14026+4341	0.323	16.5	0.62	0.459	12.86	2.3	−24.4	–	0.260
18508−7815	0.162	15.5	1.11	0.239	12.34	7.8	−23.7	–	0.174
21219−1757	0.112	14.8	1.07	0.418	12.04	4.7	−23.6	1.7	0.255
Z05558−5008	0.355	16.3	0.16	0.563	12.15L	1.8L	−24.8	0.4	0.227L
Z06367−6845	0.336	16.0	0.18	0.333	12.43	3.1	−25.0	0.8	0.156
F21382−2659	0.129	14.6	0.24	1.083	11.93L	2.2L	−24.1	2.1	0.241L

[a] $R = F$(25 μm)/F(60 μm) and $F_{\rm IR} = 1.8 \times 10^{-14} X$, where $X = [13.48F(12) + 5.16F(25) + 2.58F(60) + F(100)]$ (see Sanders & Mirabel 1996).
[b] $L(25)/L_{\rm IR} = 5.16F(25)/X$ and $H_0 = 75$ km s^{-1}Mpc^{-1}, $q_0 = 0$.
[c] L indicates a lower limit.

the 12–100 μm range. As the 12 quasars were not selected because of their strong 25-μm emission, this is not too surprising: the only source not following this trend is IRAS 13349+2438, which, from our earlier discussion, we know to be an exceptional source with very strong 25-μm emission. The three quasars plus IRAS 13349+2438 appear to define significantly different SEDs.

For two of the three quasars for which we have AAT images, IRAS F21382−2659 and Z06367−6845, we suspect that there may be a faint, close companion galaxy. The possibility that galaxy interactions may be the source of material that either triggers or continues to feed the nuclear activity in quasars has been discussed for over a decade (see e.g. Stockton 1990; Hutchings & Neff 1992). Bahcall et al. (1997) using *HST* images have found at least one companion for two-thirds of their sample of 20 quasars, which if they are proved to be true companions would lie within 25 kpc of each quasar. Spectroscopy of close (< 3 arcsec) companions to three different quasars by Canalizo & Stockton (1997) confirmed that two out of three were true companions. *HST* images (Planetary Camera) of three of the 12 *IRAS* quasars discussed above (Boyce et al. 1996) clearly reveal interactions in at least two and perhaps all three of the objects. Sanders et al. (1988) believe that the *IRAS* quasars represent an intermediate stage between mergers, which in their early stages are observed as ultraluminous *IRAS* galaxies, and classical quasars, and that the buried quasar emerges as the dust from the merger process is gradually blown away. According to Boyce et al. (1996) their *HST* images imply that the quasars 04505−2958, 07598+6508 and 13218+0552 are young and not emerging from their dust shrouds in the late stages of the merger/interaction process: they argue that we are seeing the optical radiation through holes in the shroud.

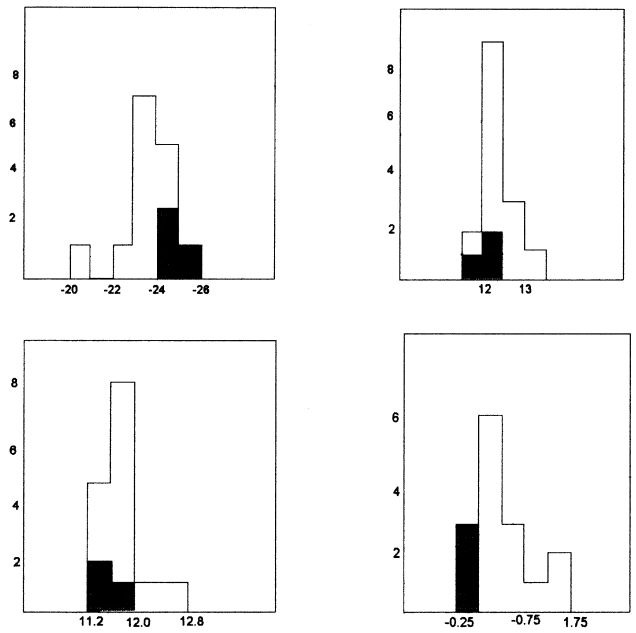

Figure 11. Histograms of $M(B)$, $\log(L_{IR}/L_{\odot})$, $\log[L(25)/L(B)]$ and $\log[L(25)/L_{\odot}]$ (shown clockwise from the upper left) for the 12 previously known *IRAS* quasars and the three new quasars described in this paper (see Table 8).

It appears from the above that *IRAS* quasars undergoing interactions may represent the norm rather than the exception (for further evidence see Hutchings & Morris 1995; Canalizo & Stockton 1997). If it is true that the shroud is pierced somewhat randomly by a wind that permits a nuclear searchlight to escape and reach us either directly or via scattering, then this could affect the optical polarization in an unpredictable manner. If there is just one escape route through the shroud, this is unlikely to be directed at the observer, and so any light reaching us would be scattered and hence polarized: such objects would most probably have high $L_{IR}/L(B)$ such as IRAS 09104+4109, 12540+5708 and 13218+0552: the first two of these have measured values of optical polarization, both high (14.8 and 7.3 per cent). On the other hand the polarization may have no connection with the geometry of a wind-pierced shroud and may be more conventionally related to the geometry of an AGN hidden by a dusty torus, e.g. as argued by Hines & Wills (1995) for IRAS 07598+6508. At present it seems unlikely that the polarization can be used as a reliable tool to gain geometrical insights into individual *IRAS* quasars, even if *IRAS* quasars are truly a group of physically similar monsters.

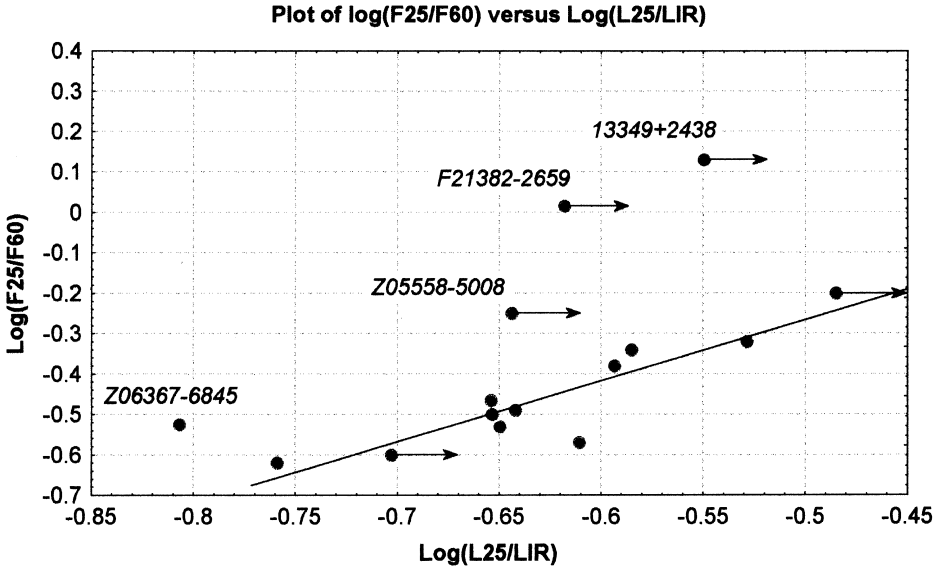

Figure 12. The dependence of the ratio $F(25\,\mu m)/F(60\,\mu m)$ on $L(25)/L_{IR}$ for the objects in Table 7.

ACKNOWLEDGMENTS

We are grateful to Gavin Ramsay and Mark Cropper, to Dick Hunstead and Gordon Robertson, and to David Buckley and Patricia Whitelock, for their valuable contributions on the AAT, MOST and SAAO telescopes, respectively. We also acknowledge useful comments and suggestions by an anonymous referee that have helped to improve this paper.

REFERENCES

Antonucci R., 1993, ARA&A, 31, 473
Bahcall J. N., Kirharos S., Saxe D. H., Schneider D. P., 1997, ApJ, 479, 642
Baldwin J., Ferland G., Korista K., Verner D., 1995, ApJ, 455, L119
Beichman C. A., Soifer B. T., Helou G., Chester T. J., Neugebauer G., Gillett F. C., Low F. J., 1986, ApJ, 308, L1
Boroson T. A., Green R. F., 1992, ApJS, 80, 109
Bowen D. V., Blades J. C., Pettini M., 1995, ApJ, 448, 634
Boyce P. J. et al., 1996, ApJ, 473, 760
Canalizo G., Stockton A., 1997, ApJ, 480, L5
Clowes R. G., Leggett S. K., Savage A., 1991, MNRAS, 250, 597
Conrow T. et al., 1993, BAAS, 25, 1291
de Grijp M. H. K., Miley G. K., Lub J., de Jong T., 1985, Nat, 314, 240
de Grijp M. H. K., Keel W. C., Miley G. K., Goudfrooij P., Lub J., 1992, A&AS, 96, 389
Done C., Krolik J. H., 1996, ApJ, 463, 144
Efstathiou A., Rowan-Robinson M., 1995, MNRAS, 273, 649
Eracleous M., Halpern J. P., 1994, ApJS, 90, 1
Ferguson J. W., Korista K. T., Baldwin J. A., Ferland G. J., 1997, ApJ, 487, 122
Granato G. L., Danese L., 1994, MNRAS, 268, 235
Hines D. C., Wills B. J., 1995, ApJ, 448, L69
Hutchings J. B., Morris S. C., 1995, AJ, 109, 1541
Hutchings J. B., Neff S. G., 1992, AJ, 104, 1
Jackson N., Browne I. W. A., 1989, MNRAS, 236, 97
Keel W. C., de Grijp M. H. K., Miley G. K., Zheng W., 1994, A&A, 283, 791
Kotilainen J. K., Ward M. J., Boisson C., de Poy D. L., Smith M. G., 1992, MNRAS, 256, 149
Lawrence A., Saunders W., Rowan-Robinson M., Crawford J., Ellis R. S., Frenk C. S., Efstathiou G., Kaiser N., 1988, MNRAS, 261
Lawrence A., Elvis M., Wilkes B. J., McHardy I., Brandt N., 1997, MNRAS, 285, 879
Lipari S., Macchetto F., Golombek D., 1991, ApJ, 366, L65
Lipari S., Terlevich R., Macchetto F., 1993, ApJ, 406, 451
Low F. J., Huchra J. P., Kleinmann S. G., Cutri R. M., 1988, ApJ, 327, L41
Low F. J., Cutri R. M., Kleinmann S. G., Huchra J. P., 1989, ApJ, 340, L1
Mathewson D., Ford V., 1970, Mem. R. Astron. Soc., 74, 139
Miley G. K., Neugebauer G., Soifer B. T., 1985, ApJ, 293, L11
Moorwood A. F. M., Oliva E., 1994, in Kneubuhl F. K., ed., Topical Conference on Infrared Astrophysics, Infrared Phys. Technol. Vol. 35, p. 349
Osterbrock D. E., 1989, Astrophysics of Gaseous Nebulae and Active Galactic Nuclei. University Science Books, Mill Valley, CA
Parker Q. A., 1997, in Kontizas E., Kontizas M., Morgan D. H., Vettolani G, eds, Astrophysics and Space Science Library, vol. 212. Kluwer, Dordrecht, p. 25
Peterson B. M., 1993, PASP, 105, 247
Pier A., Krolik J., 1992, ApJ, 401, 99
Pier A., Krolik J., 1993, ApJ, 418, 673
Robinson A., 1995a, MNRAS, 272, 647
Robinson A., 1995b, MNRAS, 276, 933
Sanders D. B., Mirabel I. F., 1996, ARA&A, 34, 749
Sanders D. B., Soifer B. T., Elias J. H., Madore B. F., Matthews K., Neugebauer G., Scoville N. Z., 1988, ApJ, 325, 74
Scarrott S. M., Warren-Smith R. F., Pallister W. S., Axon D. J., Bingham R. G., 1983, MNRAS, 204, 1163
Shields J. C., Ferland G. J., Peterson B. M., 1995, ApJ, 441, 507
Shuder J. M., 1982, ApJ, 259, 48
Shuder J. M., 1984, ApJ, 280, 491
Stirpe G. M., 1990, A&A, 240, 564
Stockton A., 1990 in Wielen R., ed., Dynamics and Interactions of Galaxies. Springer-Verlag, Berlin, p. 440
Storchi-Bergmann T., Eracleous M., Livio M., Wilson A. S., Filippenko A. V., Halpern J. P., 1995, ApJ, 443, 617
Storchi-Bergmann T., Eracleous M., Ruiz M. T., Livio M., Wilson A. S., Filippenko A. V., 1997, ApJ, 489, 87
Urry C. M., Padovani P., 1995, PASP, 107, 803
Ward M. J., Blanco P. R., Wilson A. S., Nishida M., 1991, ApJ, 382, 115
Wills B. J., Wills D., Evans N. J., Natta A., Thompson K. L., Breger M., Sitko M. L., 1992, ApJ, 400, 96
Wolstencroft R. D., Savage A., Clowes R. G., MacGillivray H. T., Leggett S. K., Kalafi M., 1986, MNRAS, 223, 279

This paper has been typeset from a TEX/LATEX file prepared by the author.